

Macroturbulent Equilibration in a Thermally Forced Primitive Equation System

MALTE JANSEN AND RAFFAELE FERRARI

Massachusetts Institute of Technology, Cambridge, Massachusetts

(Manuscript received 27 January 2011, in final form 22 August 2011)

ABSTRACT

A major question for climate studies is to quantify the role of turbulent eddy fluxes in maintaining the observed ocean–atmosphere state. It has been argued that eddy fluxes keep the midlatitude atmosphere in a state that is marginally critical to baroclinic instability, which provides a powerful constraint on the response of the atmosphere to changes in external forcing. No comparable criterion appears to exist for the ocean. This is particularly surprising for the Southern Ocean, a region whose dynamics are very similar to the midlatitude atmosphere, but observations and numerical models suggest that the currents are supercritical.

This paper aims to resolve this apparent contradiction using a combination of theoretical considerations and eddy-resolving numerical simulations. It is shown that both marginally critical and supercritical mean states can be obtained in an idealized diabatically forced (and thus atmosphere-like) Boussinesq system, if the thermal expansion coefficient is varied from large atmosphere-like values to small oceanlike values. The argument is made that the difference in the thermal expansion coefficient dominantly controls the difference in the deformation scale between the two fluids and ultimately renders eddies ineffective in maintaining a marginally critical state in the limit of small thermal expansion coefficients.

1. Introduction

The response of the atmosphere and ocean circulations to changes in the external forcing is a crucial question for studies of climate and climate change. A major difficulty in answering this question is that the response of the mean circulation is strongly affected by changes in the macroturbulence in the two fluids. Heuristic arguments have been put forward to predict the turbulent adjustment to changes in the external forcing, both for the atmosphere and the ocean. Surprisingly the arguments put forward for the two fluids are remarkably different, despite the dynamical similarities between the two fluids. The goal of this paper is to revisit the heuristic arguments developed for the atmosphere and explore in which parameter range they hold.

The nature of the turbulent fluxes changes with the medium and the latitude under consideration. In the tropical atmosphere, the saturated moist entropy is well mixed in the vertical: this well-homogenized state is marginally

critical to convective instability and turbulence acts to maintain the system in equilibrium. The implication is that whatever the changes in external forcing, the turbulent fluxes will respond so as to keep saturated moist entropy homogeneous. The problem is more complex in the midlatitude atmosphere, since the turbulent fluxes originate from baroclinic instabilities of the mean jets and redistribute entropy and momentum both in the horizontal and in the vertical. There is no agreed-upon theory as to how baroclinic jets equilibrate and this is the topic of the present paper. A common argument is that, in analogy to the tropical problem, the turbulent eddy fluxes keep the midlatitude atmosphere in a state that is marginally critical to baroclinic instability. The prediction has some observational support in the atmosphere (Stone 1978), although the generality of the argument has been challenged by some numerical studies (e.g., Panetta and Held 1988; Thuburn and Craig 1997; Barry et al. 2000; Zurita-Gotor 2008). Most puzzling is the fact that the marginal criticality condition is not satisfied in the Southern Ocean, even though this ocean is characterized by a reentrant baroclinically unstable current and is dynamically very similar to the midlatitude atmosphere. Yet, the failure of the marginal criticality argument for the ocean has not received much attention.

Corresponding author address: Malte Jansen, Massachusetts Institute of Technology, 77 Massachusetts Avenue, 54-1615, Cambridge, MA 02139.
E-mail: mfjansen@mit.edu

The original argument for baroclinic adjustment, made by Stone (1978), is based on the condition for marginal criticality in the two-layer quasigeostrophic (QG) model, which can be written as

$$\xi_{\text{QG}} \equiv \frac{fs}{\beta H} = 1, \quad (1)$$

where ξ_{QG} is the criticality parameter, H is the lower layer depth, s is the slope of the interface, f is the Coriolis parameter, and $\beta = \partial_y f$. Condition (1) states that the QG potential vorticity (PV) gradient in the lower layer vanishes because of a cancellation between the planetary vorticity gradient β and the “thickness” gradient fs/H . If H is assumed to scale as the tropopause height and s is the isentropic slope in the atmosphere, then condition (1) predicts that in a marginally critical state isentropes leaving the surface in the subtropics will reach the tropopause at about the pole, which is in general agreement with the observed state of the atmosphere. The argument is very appealing, but it is not clear to what extent the condition for baroclinic instability can be applied to continuously stratified models. Held (1978, 1982), derives a similar result for a continuously stratified QG model, assuming that the height of the troposphere is given by the vertical extent of eddy fluxes in Charney-type instabilities; and Schneider (2004), argues that a similar constraint can be obtained based on a relation between eddy fluxes of potential vorticity and surface potential temperature in a primitive equation (PE) system. These results do not explicitly depend on a criticality condition to baroclinic instability, suggesting that the marginal criticality scaling in Eq. (1) is more general than implied by the baroclinic instability argument.

An important implication of the limitation of the criticality parameter to order one is that turbulence cannot produce a significant upscale energy transfer. The latter relies upon a separation between the deformation scale, at which turbulent eddies are generated through baroclinic instability of the mean state, and the halting scale, which has to be larger than the scale of the instability. Held and Larichev (1996), using the two-layer QG model, show that such a scale separation is contingent on ξ_{QG} being larger than one. In agreement with the observation that the criticality parameter is close to one, no significant separation between the scale of the instability and the halting scale appears to exist in the atmosphere (e.g., Merlis and Schneider 2009, and references therein).

The marginal criticality arguments reviewed above are quite general and should apply to baroclinic jets both in the atmosphere and in the ocean. The Southern Ocean

is a good test case because it is characterized by an uninterrupted circumpolar jet, the Antarctic Circumpolar Current (ACC), whereas ocean flows at other latitudes are blocked laterally by continents, resulting in a different equilibration problem. Analogous to the mid-latitude atmosphere, dynamic fluxes of entropy and momentum are here dominated by turbulent eddies arising from baroclinic instability of the mean state (e.g., Karsten and Marshall 2002, and references therein). One should therefore expect the arguments for baroclinic adjustment to hold in the ACC region. However, observations and numerical models of the Southern Ocean show that the ACC region is supercritical, with QG PV gradients much larger than β , and also displays an upscale energy transfer due to nonlinear eddy–eddy interactions (Scott and Wang 2005; Tulloch et al. 2011). The motivation for this paper is to resolve this apparent contradiction using theoretical arguments as well as idealized numerical simulations.

When comparing ocean and atmospheric jets, two differences are most apparent. First, the ocean is primarily driven mechanically by surface wind stresses, while the atmosphere is a heat engine driven by differential heating throughout the troposphere (e.g., Wunsch and Ferrari 2004). Second, the two fluids have different properties (density, compressibility, etc.). This paper will focus on the second difference and will show that by varying fluid properties it is possible to obtain atmosphere-like marginally critical states, as well as more oceanlike supercritical states.

We will consider an idealized, thermally forced (and thus atmosphere-like) Boussinesq system. Within the idealized framework of a Boussinesq fluid, differences in the fluid properties between air and water are captured by the very different thermal expansion coefficients. We will therefore consider a thermally forced channel with thermal expansion coefficients spanning from atmospheric (air) to oceanic (water) values. It will be shown that eddies become ineffective at maintaining the system in a marginally critical state in the oceanlike limit of small thermal expansion coefficients.

The role of the thermal expansion coefficient in setting dynamical properties of the system will be discussed in section 2. In section 3 we introduce a theoretical framework for the eddy equilibration of an idealized thermally forced Boussinesq system, using primitive equations in isentropic coordinates. In section 4 we present a series of numerical simulations using a diabatically forced primitive equation model in a channel configuration. It is shown that marginally critical as well as supercritical states can be found simply by varying the thermal expansion coefficient. A summary and discussion of the results are offered in section 5.

2. Representation and implications of fluid properties in an idealized Boussinesq framework

We idealize the problem of turbulent adjustment by considering a Boussinesq fluid in a thermally forced zonally reentrant channel. This configuration maintains all the physics that are essential to test the ideas discussed in the introduction, while omitting some of the complicating factors found in real geophysical fluids. In particular, it allows us to continuously vary fluid properties from atmospheric to oceanic values, without changing the dynamical equations.

Fluid differences enter the dynamical equations only via the equation of state, which in the Boussinesq system becomes an equation for buoyancy. Consistent with the Boussinesq approximation, buoyancy is assumed to depend linearly on potential temperature only, that is,

$$b = g\alpha(\theta - \theta_0), \tag{2}$$

where θ_0 is some reference potential temperature and $\alpha = -(1/\rho)(\partial\rho/\partial\theta)$ is the thermal expansion coefficient. Within the Boussinesq approximation, the differences between air and water are thus captured by α (the dynamics depends only on gradients of buoyancy and are thus independent of the reference potential temperature θ_0). For typical oceanic conditions the thermal expansion coefficient is about $\alpha \approx 1-3 \times 10^{-4} \text{ K}^{-1}$. For a dry atmosphere, where the equation of state is well approximated by the ideal gas law, on the other hand,

$$\alpha = -\frac{1}{\rho} \frac{\partial\rho}{\partial\theta} = \frac{1}{\theta} \approx 3.6 \times 10^{-3} \text{ K}^{-1}, \tag{3}$$

where we assumed a typical potential temperature $\theta \approx 280 \text{ K}$. The thermal expansion coefficient of air is thus about 10–40 times bigger than that of ocean water. Since planetary-scale potential temperature contrasts are of similar order in the atmosphere and ocean (because of the strong coupling between the two fluids), the much larger thermal expansion coefficient causes buoyancy contrasts to be about 10–40 times larger in the atmosphere, resulting in much stronger circulations.

As discussed in the introduction, one of the key differences between the midlatitude atmosphere and the Southern Ocean is the different deformation scales, which are largely set by the different thermal expansion coefficients of the two fluids. Assuming that the stratification is approximately constant in the vertical, and using the linear equation of state [Eq. (2)], the deformation radius scales as

$$L_d \sim \frac{\sqrt{\Delta_v b H}}{f} \sim \frac{\sqrt{g\alpha\Delta_v\theta H}}{f}, \tag{4}$$

where $\Delta_v b$ and $\Delta_v\theta$ denote the vertical buoyancy and potential temperature differences and H is the depth of

the troposphere or the thermocline. The vertical temperature differences are of the same order as the horizontal ones, and they are of the same order in the atmosphere and ocean. Hence the differences in the deformation radii between the atmosphere and the ocean arise from two main parameters: the large differences in the thermal expansion coefficients and the different depth scales. Specifically, α is about 10–40 times larger in the atmosphere than in the ocean, while H is about 10 km for the troposphere but only about 1 km for the ocean’s thermocline. Together these differences account for the observation that the deformation scale of the atmosphere is larger than that of the ocean by a factor of $\sqrt{100} - \sqrt{400} \sim 10 - 20$.

3. Macroturbulent adjustment in an isentropic framework

We introduce a theoretical framework to address the question of how macroturbulence sets the equilibrated thermal structure of a thermally forced primitive equation system. The discussion will be presented in the framework of the full primitive equations expressed in isentropic coordinates. A simplified derivation based on the QG approximation is given in appendix A. While the QG-based discussion has some obvious shortcomings, it captures the essence of the results derived below. On a first reading, one might therefore skip to appendix A and then proceed directly to the numerical simulations discussed in section 4.

We will first discuss dynamical constraints on the zonal momentum balance inspired by the work of Koh and Plumb (2004) and Schneider (2004, 2005). Departing from Schneider (2004), who integrates the zonal momentum budget over the whole depth of the troposphere, we will integrate only to the top of the surface layer (SL)—that is, that part of the atmosphere that includes all isentropes that intersect with the surface at some longitude or time, as sketched in Fig. 1. (The reasons for this will be discussed later.) To close the SL momentum budget we will derive an additional constraint for the total meridional mass transport in the SL. Armed with these two constraints, we will be able to relate the turbulently adjusted mean state to the radiative forcing. For simplicity all arguments and simulations presented here assume a Boussinesq fluid in a flat-bottomed reentrant channel configuration. Notice, however, that the same qualitative results are obtained for an ideal gas atmosphere on a spherical planet.

a. Dynamical constraint: The zonal momentum balance

We start with the vertically integrated temporal- and zonal-mean isentropic zonal momentum balance discussed

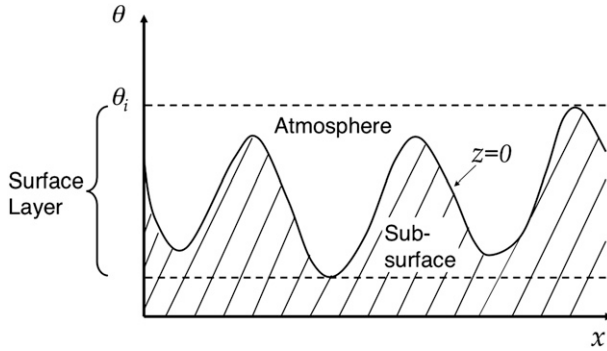


FIG. 1. Sketch of the surface layer (SL). The undulating bottom surface of the atmosphere shown in the longitude–potential temperature (x, θ) plane. The SL comprises all isentropes that intersect with the surface at some longitude and time.

in Schneider (2005). For a Boussinesq fluid in a statistically steady state in the limit of small Rossby numbers (appropriate for large-scale ocean and atmospheric flows), this can be approximated as

$$\int_{b_{\min}}^{b_i} \overline{h_b v^*} db \approx - \int_{b_{\min}}^{b_i} \frac{\overline{h_b \hat{v} P^*} + \overline{h_b J_F^*}}{\overline{P^*}} db - \frac{f}{\overline{P^*}(\overline{b_s^s})} \overline{v'_{gs} b_s'^s}, \quad (5)$$

where v is the full meridional velocity and v_{gs} is the meridional geostrophic velocity at the surface, b is buoyancy, b_s the surface buoyancy, b_{\min} the minimum buoyancy in the domain, and b_i a buoyancy level above the SL. Also, $h_b = \mathcal{H}(b - b_s) \partial_b z$ is the isentropic thickness and z is the height of the isentrope b . The thickness is multiplied by the Heaviside function \mathcal{H} so that it vanishes when isentropes intersect the ground. The potential vorticity is $P = f/\partial_b z$, consistent with the small Rossby number assumption, while J_F^* represents frictional forces. The overbar denotes an isentropic zonal and temporal average, $(\cdot)^* = \overline{h_b(\cdot)}/\overline{h_b}$ is the thickness weighted zonal average, and (\cdot) denotes a zonal and temporal average along the surface. Primes denote departures from the zonal averages and hats denote departures from the thickness weighted averages.

Equation (5) looks similar to its QG analog: Eq. (A2) derived in appendix A by averaging the zonal QG momentum budget. It states that the net volume transport (or “residual transport”) between the surface and the isentropic surface b_i is driven by the interior meridional PV flux $\hat{v} P^*$ and the surface geostrophic buoyancy flux $v'_{gs} b_s'^s$. Hence, QG theory can be used to qualitatively understand the momentum budget of a baroclinic jet. There are, however, important quantitative differences between the PE and QG budgets. In QG, the SL is

infinitesimally thin and contributes only the buoyancy flux, while the PV flux acts only in the interior. In PE, the SL spans up to half of the troposphere in the real atmosphere (e.g., Schneider 2004). In particular, the surface buoyancy flux represents the eddy form drag generated by outcropping isentropes in the SL.

To transform Eq. (5) into a constraint for the mean variables, we need a closure for the eddy fluxes of PV and surface buoyancy. Mixing length arguments (Rhines and Young 1982) and numerical studies (e.g., Pavan and Held 1996) suggest that the eddy fluxes are down their mean gradients, such that

$$\overline{\hat{v} P^*} = -D \partial_y \overline{P^*}, \quad \overline{v'_{gs} b_s'^s} = -D \partial_y \overline{b_s^s}, \quad (6)$$

with an eddy diffusivity D that, for simplicity, is here assumed constant in the vertical. As discussed in appendix B, all the key relationships derived below are recovered if we allow for vertical variations in the eddy diffusivity, with D replaced by a bulk eddy diffusivity that tends to be dominated by its near-surface value. Ignoring frictional forces, which are small in the atmosphere (Schneider 2005), the isentropic mass flux Eq. (5) becomes

$$\int_{b_{\min}}^{b_i} \overline{h_b v^*} db \approx D \int_{b_{\min}}^{b_i} \frac{\overline{h_b \partial_y P^*}}{\overline{P^*}} db + \frac{f}{\overline{P^*}(\overline{b_s^s})} D \partial_y \overline{b_s^s}. \quad (7)$$

Using the facts that $P = f/\partial_b z$ and $h_b = \mathcal{H}(b - b_s) \partial_b z$, the thickness-weighted average of PV can be written as $\overline{P^*} = \overline{h_b P}/\overline{h_b} \approx \mathcal{H}(b - b_s) f/\overline{h_b} = \Pi f/\overline{h_b}$, where $\Pi = \mathcal{H}(b - b_s)$ denotes the fraction of the isentrope that is above the surface.¹ We can now rewrite the first term on the rhs of Eq. (7) as

$$\begin{aligned} \int_{b_{\min}}^{b_i} \frac{\overline{h_b \partial_y P^*}}{\overline{P^*}} db &\approx \int_{b_{\min}}^{b_i} \left(\frac{\overline{h_b \beta}}{f} - \partial_y \overline{h_b} + \frac{f}{\overline{P^*}} \partial_y \Pi \right) db \\ &= \frac{\beta}{f} \overline{z}(b_i) - \partial_y \overline{z}(b_i) - \frac{f}{\overline{P^*}(b_s)} \partial_y b_s \\ &\approx \frac{\beta}{f} \overline{z}(b_i) - \partial_y \overline{z}(b_i) - \frac{f}{\overline{P^*}(\overline{b_s^s})} \partial_y \overline{b_s^s}. \end{aligned} \quad (8)$$

¹ Notice that we here use the PV definition used by Koh and Plumb (2004) or “convention II” discussed by Schneider (2005). However, if it is assumed that the isentropic slope varies little over the depth of the SL, “convention I” of Schneider (2005) yields a result very similar to Eq. (9) except for an additional factor of $3/2$ in front of the slope on the rhs. Notice however that, as will be discussed below, the differences do become crucial if the integration is taken over the whole depth of the tropopause instead of over just the SL, as done in Schneider (2004).

The approximation in the last step can be formalized by expanding variables around \bar{b}_s , following a similar derivation for the surface buoyancy flux term sketched in Schneider [2005, his Eq. (11)]. Using the relationship in Eq. (8), Eq. (7) can now be written as

$$\Psi_Q(b_i) \approx D \left[s(b_i) - \frac{\beta}{f} \bar{z}(b_i) \right], \quad (9)$$

where $s(b_i) = \partial_y \bar{z}(b_i)$ denotes the slope of the isentrope b_i and $\Psi_Q(b_i) \equiv -\int_{b_{\min}}^{b_i} \bar{h} \bar{v}^* db$ is the isentropic overturning streamfunction (the subscript Q reminds us that Ψ_Q is related to the diabatic forcing Q , as discussed below).

Equation (9) states that the net isentropic mass transport in the SL is proportional to the eddy diffusivity times an effective SL PV gradient, which is given by the sum of the vertical integral of the planetary vorticity gradient and the isentropic slope at the top of the SL. This effective SL PV gradient is similar to the PV gradient in the bottom layer of a layered QG model, supporting the interpretation that the lower layer of a two-layer QG model might be regarded as representative of the SL. Note, however, that the vertical extent of the SL is not fixed (as in a layered QG model) but can adjust (e.g., to changes in the forcing).

Notice that our approach differs from that of Schneider (2004), who stretched the integral in Eq. (7) all the way to the tropopause, where $\Psi_Q(b_t) = 0$ by definition, and obtained the condition that the criticality parameter has to be close to one. However, the result obtained by integrating Eq. (7) all the way to the tropopause depends crucially on assumptions for computing PV on isentropes below the surface [which Schneider (2005) refers to as “conventions I and II”] and on the vertical structure of the eddy diffusivity under the respective conventions. By integrating Eq. (7) only over the SL, our result does not depend on these somewhat arbitrary “conventions” or on the exact vertical structure of the eddy diffusivity.

In the limit of weak diabatic circulation (i.e., $|\Psi_Q/D| \ll |s(b_i)|$), relation (9) simplifies to a statement analogous to the marginal criticality condition of the two-layer QG model, with the layer depth given by the depth of the SL: that is,

$$\frac{fs(b_i)}{\beta \bar{z}(b_i)} \approx 1. \quad (10)$$

Similar to the marginal criticality condition of the two-layer QG model, Eq. (10) states that the effective PV gradient integrated over the SL has to vanish. The SL thus becomes the analog to the lower layer in the two-layer QG model. The relevance of this limit for typical

atmospheric conditions will, however, be questioned in the following section, where we will derive a scaling for the diabatic circulation Ψ_Q and show that Ψ_Q/D is typically not small compared to $s(b_i)$.

b. Thermodynamic constraint: Isentropic mass budget

A relation between the isentropic mass transport and the diabatic forcing can be derived from the time- and zonal-mean continuity equation in isentropic coordinates:

$$\partial_y(\bar{h}_b v) + \partial_b(\bar{h}_b Q) = 0, \quad (11)$$

where $Q = db/dt$ denotes the diabatic forcing. Equation (11) can be integrated meridionally and vertically to yield

$$\Psi_Q(y, b_i) \equiv -\int_{b_{\min}}^{b_i} \bar{h}_b v(y, b') db' = \int_{y_s}^y \bar{h}_b Q(y', b_i) dy', \quad (12)$$

where we used the fact that h_b vanishes on subsurface isentropes and thus $\bar{h}_b Q(y, b_{\min}) = 0$ for all y . Here y_s denotes the southernmost latitude where the isentrope b_i intersects with the surface or with the southern boundary of the channel if it does never intersect the surface (see sketch in Fig. 2).

By integrating Eq. (12) from y_s to the northern boundary of the domain y_{\max} , we can further show that in equilibrium the net heating along an isentrope has to vanish, so we can replace the diabatic heating in the SL by the diabatic cooling above. We thus have

$$\begin{aligned} \Psi_Q(y, b_i) &= \int_{y_s}^y \bar{h}_b Q(y', b_i) dy' = -\int_y^{y_{\max}} \bar{h}_b Q(y', b_i) dy' \\ &\approx -\int_y^{y_t} \bar{h}_b Q(y', b_i) dy', \end{aligned} \quad (13)$$

where $y_t(b_i)$ denotes the latitude at which b_i intersects with the tropopause. Equation (13) is derived assuming that the net heating over a certain buoyancy class $\bar{h}_b Q$ is negligible above the tropopause, an assumption equivalent to assuming that the isentropic mass transport is small above the tropopause, which is confirmed in the simulations discussed below and in atmospheric analysis (e.g., Bartels et al. 1998, their Fig. 1). If b_i is chosen to be the buoyancy just above the SL, the relationship in Eq. (13) implies that the overturning $\Psi_Q(b_i)$ at the top of the SL is given by the integrated cooling along b_i above the SL. This cooling must be balanced by a similar warming within the SL. Thus, Ψ_Q is given by the total

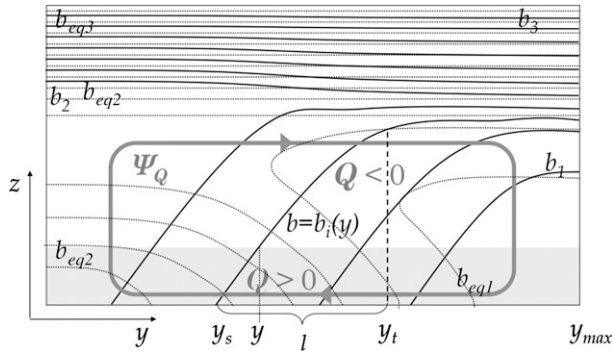


FIG. 2. Sketch of the diabatically driven overturning circulation Ψ_Q . The solid and dotted lines denote isentropes of the mean and radiative equilibrium states, respectively, with $b_3 = b_{eq3} > b_2 = b_{eq2} > b_1 = b_{eq1}$. The shading indicates the surface layer, which at latitude y extends up to the buoyancy $b = b_i(y)$. Note that the net heating and cooling integrated along the isentrope b_i over the distance l (i.e., from its intersection with the surface to its intersection with the tropopause) approximately vanishes (see section 3b).

amount of heat transported out of the SL and into the interior within the buoyancy class b_i .

Equation (13) can now be used to derive a scaling for the diabatic overturning streamfunction. Let us assume that the diabatic forcing can be represented by a radiative relaxation—that is, $Q \sim -(b - b_{eq})/\tau_r$ with a restoring time scale τ_r to an equilibrium buoyancy b_{eq} . This is indeed the form of radiative forcing used in the simulations described below and in many idealized studies of the atmosphere (e.g., Held and Suarez 1994; Schneider 2004). Using Eq. (13) we can then argue that

$$\Psi_Q \sim \frac{\Delta b_{eq} l}{\tau_r \partial_z \bar{b}}, \quad (14)$$

where l is the meridional length of the isentrope b_i , and Δb_{eq} denotes the variation of the equilibrium buoyancy along the isentrope b_i (see Fig. 2 for a sketch). Relation (14) assumes that the radiative imbalance $b - b_{eq}$ along each isentrope above and below the top of the SL scales with the variation of the radiative equilibrium buoyancy along the respective isentrope Δb_{eq} ; this is derived in detail in appendix C. Note that Δb_{eq} is not fixed but rather depends on the mean state and in particular on the isentropic slope. However, changes in Δb_{eq} are small across all the simulations discussed in this paper.

c. Implications for the equilibrium state and criticality

The scaling for Ψ_Q can be used to show that condition (10) (which can be viewed as a generalization of the QG

marginal criticality condition, with the layer depth replaced by the depth of the SL) cannot be expected to hold generally. The requirement for Eq. (10) to hold is that $\Psi_Q/Ds(b_i) \ll 1$, which with Eq. (14) becomes

$$\frac{\Psi_Q}{Ds(b_i)} \sim \frac{\Delta b_{eq} l}{D\tau_r \partial_y \bar{b}} \sim \frac{\Delta b_{eq} l^2/D}{\Delta_y \bar{b} \tau_r} \ll 1. \quad (15)$$

Here $\Delta_y \bar{b} \sim l \partial_y \bar{b}$ denotes the horizontal buoyancy difference over the meridional extent l of the isentrope b_i (note that the y derivative is here taken at constant z). Generally $\Delta b_{eq} \gtrsim \Delta_y \bar{b}$, because $\Delta b_{eq} \gtrsim \Delta_y b_{eq}$ since the vertical tilt of the isentropes adds a positive contribution to the buoyancy contrast along an isentrope (if the restoring profile is statically unstable), and $\Delta_y b_{eq} \gtrsim \Delta_y \bar{b}$ since the meridional temperature gradient is generally weaker than the temperature gradient in radiative equilibrium. Relation (15) thus implies that the diabatic term ψ_Q/D can be small only if $(l^2/D)/\tau_r \ll 1$; that is, the time scale of eddy diffusion over the length of an isentrope l^2/D has to be short compared to the restoring time scale τ_r . Equivalently, the time scale over which eddy fluxes modify the mean state needs to be fast compared to the time scale of diabatic restoring. This is not true for typical atmospheric conditions and for the numerical simulations discussed below.

In typical atmospheric conditions and in the simulations described below, the diffusive time scale is not small compared to the radiative restoring time scale. In this case the effective SL PV gradient does not vanish because $s(b_i) - \beta f^{-1} \bar{z}(b_i) \approx \psi_Q/D > 0$ for the common situation where net warming in the SL is compensated by net cooling above. This further implies that the net isentropic slope will generally be steeper than predicted by the condition $s(b_i) - \beta f^{-1} \bar{z}(b_i) = 0$ [see Eq. (10)].

Our simulations suggest that typically $fs(b_i)/\beta \bar{z}(b_i) \gg 1$ and the leading-order balance in the momentum budget [Eq. (9)] is between the diabatic overturning and the eddy diffusivity acting on the thickness gradient integrated over the SL:

$$s(b_i) \approx \frac{\Psi_Q}{D}. \quad (16)$$

Relation (16) has important implications for the criticality parameter defined as

$$\xi = \frac{fs}{\beta H_t}, \quad (17)$$

which is the form used in most studies on extratropical adjustment (e.g., Zurita-Gotor and Vallis 2011, and references therein). Here H_t denotes the depth of the

tropopause and s represents a characteristic isentropic slope (whose exact definition varies in different studies). Interpreting s as the isentropic slope at the top of the SL, Eq. (16) predicts

$$\xi \sim \frac{f}{\beta H_t} \frac{\Psi_Q}{D}, \quad (18)$$

where Ψ_Q here denotes the net mass transport over the SL, which is generally found to be close to the total overturning transport (e.g., Held and Schneider 1999). For any given planet (f/β fixed), the criticality parameter ξ thus depends on the relation between the forcing (and the associated Ψ_Q), the eddy diffusivity, and the depth of the troposphere. Baroclinic adjustment theories, which predict constant ξ , would demand that D scales as Ψ_Q/H_t . This is, however, not what we find in the numerical experiments analyzed below.

A slightly more general form of Eq. (16) can be used to compare the equilibration in atmosphere-like and oceanlike settings. If the mechanical surface stress in Eq. (5) is retained, a more general scaling for the isentropic slope is obtained:

$$s(b_i) \approx \frac{\Psi_Q - \Psi_{Ek}}{D}. \quad (19)$$

For the atmospheric case $\Psi_{Ek} \ll \Psi_Q$, which leaves us with relation (16). In a nearly adiabatic oceanic channel, on the other hand, $\Psi_Q \ll \Psi_{Ek}$, which leaves us with the scaling $s(b_i) \approx -(\Psi_{Ek}/D)$. A scaling similar to Eq. (19) is discussed in Marshall and Radko (2003) for the isentropic slope at the bottom of the mixed layer in the ACC.

4. Transition to supercritical states in a channel model

The arguments presented above are tested by analyzing numerical simulations that explicitly resolve the macroturbulence whose effect on the mean fields we are trying to understand. As in the theoretical discussion above,

we idealize the problem by considering a Boussinesq fluid in a zonally reentrant channel model.

a. Model setup

We use a hydrostatic, incompressible Cartesian coordinate configuration of the Massachusetts Institute of Technology GCM (MITgcm) (Marshall et al. 1997). The geometry is a zonally reentrant channel, 15 000 km long, bounded meridionally by sidewalls with free slip boundary conditions at $y = \pm 4500$ km, and vertically by a rigid lid at $z = H = 10.2$ km and a flat bottom at $z = 0$, with free slip and no-slip conditions, respectively. We employ a vertical viscosity of $\nu_z = 10^{-1} \text{ m}^2 \text{ s}^{-1}$ and a diffusive convective adjustment scheme with a diffusivity of $\kappa_{\text{conv}} = 10^2 \text{ m}^2 \text{ s}^{-1}$. No explicit horizontal diffusion of temperature or momentum is used, but a fourth-order Shapiro filter (Shapiro 1970) is employed to remove small-scale grid noise. The horizontal resolution for all experiments is 50 km. The vertical resolution is 400 m in the interior but refines to 50 m at the surface, adding up to a total of 29 levels. The Coriolis parameter increases linearly as

$$f = f_0 + \beta y, \quad (20)$$

where for all simulations presented $f_0 = 1 \times 10^{-4} \text{ s}^{-1}$ and $\beta = 1.6 \times 10^{-11} \text{ m}^{-1} \text{ s}^{-1}$. With this choice the Coriolis parameter varies strongly but stays positive throughout the domain. We use the linear equation of state given in Eq. (2) with varying thermal expansion coefficients.

The simulations are forced through relaxation to an equilibrium temperature profile, which is chosen to mimic some of the key features of radiative forcing in the atmosphere. The potential temperature in radiative equilibrium is specified as a function of y and z as

$$\theta_{\text{eq}} = \theta_{\text{min}} + \Delta_z \theta \left(\frac{z}{H}\right)^3 + e^{-z^2/h^2} \Delta \theta_s(y), \quad (21)$$

with $\theta_{\text{min}} = 233$ K, $\Delta_z \theta = 180$ K, and $h = 4$ km. The meridional dependence of the surface temperature is given as

$$\Delta \theta_s(y) = \begin{cases} \Delta \theta_{s0} + \Delta_y \theta & \text{for } y < -L_c \\ \Delta \theta_{s0} + \frac{\Delta_y \theta}{2} \{1 - \sin[\pi y / (2L_c)]\} & \text{for } -L_c \leq y \leq L_c \\ \Delta \theta_{s0} & \text{for } y > L_c \end{cases}, \quad (22)$$

where $\Delta \theta_{s0} = 10$ K, $\Delta_y \theta = 80$ K, and $L_c = 3500$ km. The resulting equilibrium potential temperature section is shown in Fig. 3. It is characterized by a baroclinic zone

with a width of 7000 km and an equilibrium meridional surface temperature difference of 80 K. The equilibrium potential temperature vertical gradient is everywhere

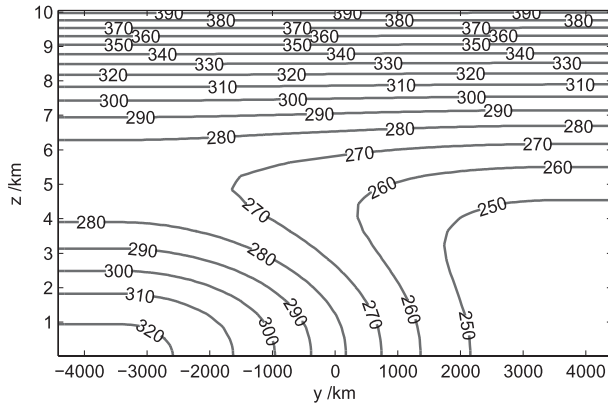


FIG. 3. Equilibrium potential temperature (K) for thermal restoring (contour interval is 10 K).

convectively unstable near the surface, while a stable radiative-equilibrium stratification is prescribed at higher altitudes to mimic the radiative effects of ozone in the stratosphere. The relaxation time scale is chosen as $\tau_{\text{int}} = 50$ days in the interior, but decreases to $\tau_s = 14$ days at the surface as

$$\tau(z)^{-1} = \tau_{\text{int}}^{-1} + (\tau_s^{-1} - \tau_{\text{int}}^{-1})e^{-(z/h_s)^2}, \quad (23)$$

with an e -folding scale $h_s = 400$ m.

All simulations are spun up until a quasi-steady state is reached and statistics are calculated as an average over at least 400 days after the equilibration is reached.

b. Results

We ran eight simulations with thermal expansion coefficients varying from $\alpha = 1.6 \times 10^{-4}$ to $1.44 \times 10^{-2} \text{ K}^{-1}$, thus spanning almost two orders of magnitudes in α and one order of magnitude in deformation radii. Note that α is varied by a factor of 2 between all “neighboring” simulations, except for the last simulation with $\alpha = 1.6 \times 10^{-4} \text{ K}^{-1}$, a value 30% smaller than the penultimate run with $\alpha = 2.25 \times 10^{-4} \text{ K}^{-1}$. Any further reduction of α would cause the deformation scale to be underresolved in the model. Notice also that for the Boussinesq equations to be an accurate description of a physical fluid we need density variations to be small, such that $|\rho - \rho_0|/\rho_0 = \alpha(\theta - \theta_0) \ll 1$, a constraint that determined the upper bound for the thermal expansion coefficient α .

Figure 4 shows surface temperature snapshots from the simulations with the smallest and largest thermal expansion coefficients, after the initial equilibration period. Both snapshots show turbulent behavior, though arguably more wavelike in the large α simulation. Also evident is a reduction of the typical eddy scale, which is

similar to the domain scale for the largest α but significantly smaller for the smallest α .

The equilibrated time- and zonal-mean states of four representative simulations with $\alpha = 2.25 \times 10^{-4}$, 9.0×10^{-4} , 3.6×10^{-3} , and $1.44 \times 10^{-2} \text{ K}^{-1}$ are shown in Fig. 5. For $\alpha \geq 3.6 \times 10^{-3} \text{ K}^{-1}$, we find that isentropes have moderate slopes, such that isentropes leaving the surface close to the southern end of the domain reach the tropopause close to the northern boundary. The baroclinic eddy kinetic energy is large over a major part of the domain and the zonal winds, which have a large barotropic component, change from westerlies in the southern part of the domain to easterlies in the north, thus implying a southward eddy flux of zonal momentum. Simulations with $\alpha \leq 9 \times 10^{-4} \text{ K}^{-1}$, on the other hand, show at least one pronounced westerly jet in the interior domain, collocated with a maximum in eddy kinetic energy (EKE). Analysis of the temporal evolution of the jets (not shown) reveals that they are largely stationary with only weak meandering. The time-mean plots in Fig. 5 are therefore qualitatively similar to the structure at any instance. The EKE, as well as the strength and the width of the jets, gets smaller as α is reduced. The reduction of kinetic energy is expected because the available potential energy (APE) in the equilibrium state decreases with α as $\text{APE} \sim \langle b''^2 \rangle H / \langle b_z \rangle \sim g\alpha \langle \theta''^2 \rangle H / \langle \theta_z \rangle$, where the angle brackets denote a domain-wide horizontal average and a double prime denotes deviations from that average.

A prominent steepening of the isentropes over the troposphere is observed for small thermal expansion coefficients, $\alpha \leq 9 \times 10^{-4} \text{ K}^{-1}$, a clear indication of changes in the criticality. This is confirmed if we compute the criticality parameter as

$$\xi \equiv \frac{f \partial_y \bar{\theta}}{\beta \Delta_V \bar{\theta}}, \quad (24)$$

where $\Delta_V \bar{\theta} \equiv \bar{\theta}(H_t) - \theta_s$ denotes a bulk stability based on the potential temperature difference between the tropopause (here defined as the height at which $d\theta/dz = 10^{-2} \text{ Km}^{-1}$) and the surface.² The horizontal temperature gradient $\partial_y \bar{\theta}$ in Eq. (24) is evaluated as an average over the lower half of the troposphere. Definition (24) has the advantage that it is not sensitive to the choice of a particular level at which we evaluate the

² Isentropes tend to flatten out in the Ekman layer in our simulations (an effect arising from a combination of Ekman drag and convective adjustment). Hence we use the model temperature above this Ekman layer, at a height of about 300 m, as the “surface” temperature.

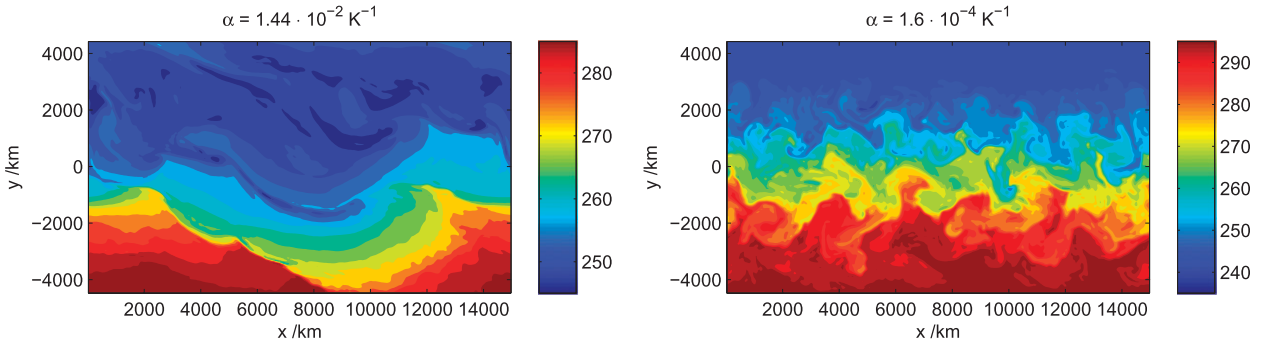


FIG. 4. Snapshots of surface potential temperature (K) for the simulations with (left) $\alpha = 1.44 \times 10^{-2}$ and (right) $\alpha = 1.6 \times 10^{-4} \text{ K}^{-1}$.

isentropic slope. The results presented here, however, do not qualitatively depend on the exact definition used for the criticality parameter.

Figure 6 shows the criticality parameter calculated as an average over the baroclinic zone between $y = -3500$ and $+3500$ km, and locally at the latitude of the maximum EKE. The domain averaged criticality parameter seems to approach a value close to one for large thermal expansion coefficients but increases steadily for values smaller than the atmosphere-like expansion coefficient $\alpha_A = 3.6 \times 10^{-3} \text{ K}^{-1}$. The criticality parameter at the latitude of maximum EKE also increases as α is decreased, but it shows a much more irregular behavior with a large jump in ξ between the simulations with $\alpha = 1.8 \times 10^{-3}$ and $9 \times 10^{-4} \text{ K}^{-1}$. Comparison with Fig. 5

shows that this jump coincides with the emergence of an interior westerly jet that is collocated with the maximum EKE.

Held and Larichev (1996) show that the criticality parameter ξ can be related to the ratio between the deformation scale, where EKE is produced by baroclinic instability, and the Rhines scale, where a possible upscale energy transfer is halted. In a marginally critical state the two scales ought therefore to be similar, resulting in no significant upscale energy transfer. We calculated the deformation scale according to

$$L_d = \frac{2}{f} \int_0^{H_1} (\partial_z \bar{b})^{1/2} dz \quad (25)$$

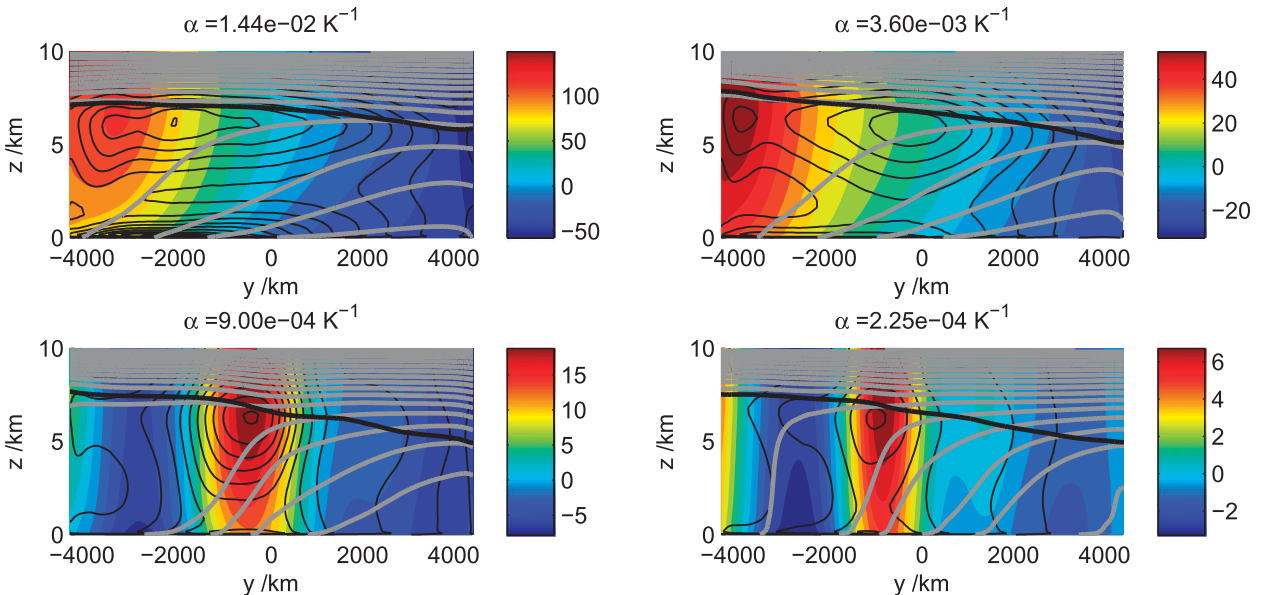


FIG. 5. Time- and zonal-mean fields of potential temperature (thick gray lines), EKE (thin black lines), zonal wind (shading; m s^{-1}) and the tropopause height, defined as the height at which $d\theta/dz = 10^{-2} \text{ K m}^{-1}$ (thick black line), for simulations with varying thermal expansion coefficients (see graph titles). The contour interval for isentropes is 10 K. Contour intervals for EKE are, from top left to bottom right, 40, 20, 10, and $3 \text{ m}^2 \text{ s}^{-2}$.

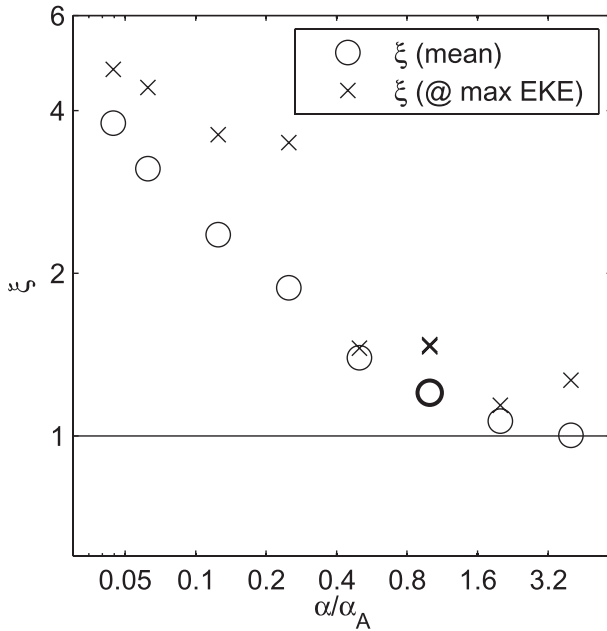


FIG. 6. Supercriticality averaged over the domain between $y = -3500$ and $+3500$ km (circles) and at the latitude of maximum EKE (crosses), as a function of the thermal expansion coefficient normalized by the atmosphere-like value of $\alpha_A = 3.6 \times 10^{-3} \text{ K}^{-1}$. The thick markers denote the simulation with an atmosphere-like thermal expansion coefficient.

(which is consistent with the Wentzel–Kramers–Brillouin (WKB) approximation for the first vertical eigenmode) and the Rhines scale as

$$L_\beta = 2\pi \frac{\text{EKE}_T^{1/4}}{\beta^{1/2}}, \quad (26)$$

where EKE_T denotes the barotropic EKE. Figure 7 shows the domain-averaged deformation and Rhines scales for all simulations. Consistent with what we found for ξ , the two scales are similar only for the experiments with the largest values of α . For smaller values of α , the deformation scale decreases much more rapidly than the Rhines scale.

The argument above assumed that 1) baroclinic instability produces EKE near the deformation scale and 2) energy is then transferred up to the Rhines scale. To test both assumptions we 1) performed a linear instability analysis and 2) calculated the eddy scale from the barotropic eddy kinetic energy spectrum.

Scales of baroclinic instability are calculated as in Smith (2007), based on the meridional planetary QG PV gradient, averaged over the domain between $y = -3500$ and $+3500$ km. For all simulations the fastest growth rates are found for a deep tropospheric eigenmode with a wavelength close to the deformation scale calculated according to Eq. (25), as shown in Fig. 7.

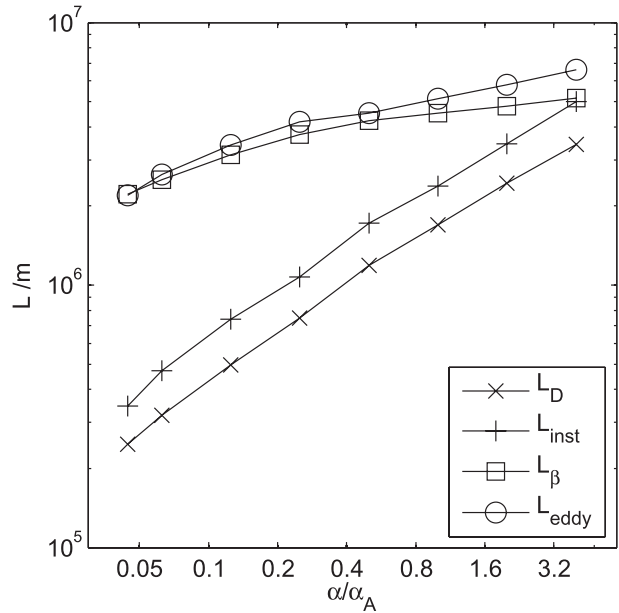


FIG. 7. Deformation scale (crosses), Rhines scale (squares), the scale of the fastest-growing wave (pluses), and the barotropic eddy scale (circles) as a function of the normalized thermal expansion coefficient α/α_A . All scales are based on averages over the domain between $y = -3500$ and $+3500$ km. See text for details.

The dominant eddy scales are estimated from the barotropic eddy kinetic energy spectra, for the same region, using a Hanning window in the meridional direction to avoid Gibbs phenomena due to nonperiodic data. The eddy scale was then calculated as the inverse centroid of the barotropic EKE spectrum as proposed by Schneider and Liu (2009)

$$L_e = 2\pi \frac{\int (k^2 + l^2)^{-1/2} E(k, l) dk dl}{\int E(k, l) dk dl}, \quad (27)$$

where $E(k, l)$ is the energy density as a function of the zonal and meridional wavenumbers. We find that the barotropic eddy scale is well approximated by the Rhines scale (Fig. 7). The results therefore suggest that, as the thermal expansion coefficient is reduced, eddies become ineffective in keeping the mean state at a criticality close to one and undergo an upscale energy transfer from the instability scale to the Rhines scale. This is confirmed by a detailed analysis of the spectral EKE budget presented in appendix D.

To compare the numerical results to the theory discussed earlier, and in particular to the prediction of Eq. (18), we need estimates for the isentropic mass transport Ψ_Q and the eddy diffusivity D . We calculated the total

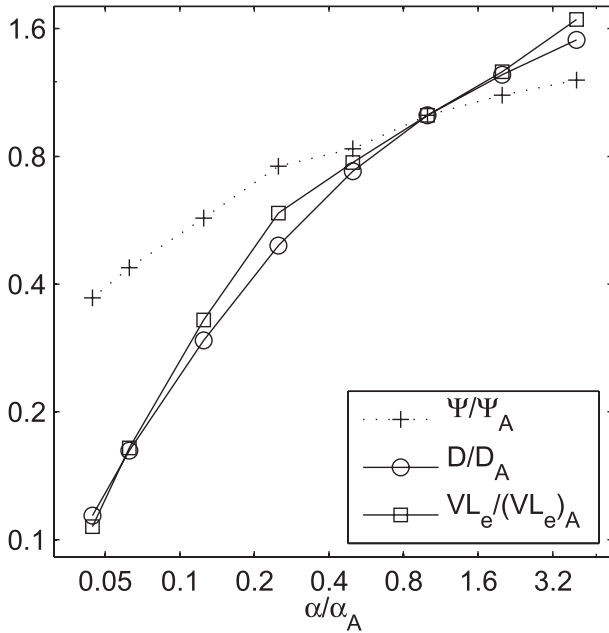


FIG. 8. Isentropic mass transport Ψ (plusses) and eddy diffusivity D estimated from a near-surface buoyancy flux–gradient relationship (circles), and from the barotropic eddy velocity and scale (squares), for varying thermal expansion coefficients. All quantities are normalized by their respective value in the simulations with $\alpha_A = 3.6 \times 10^{-3} \text{ K}^{-1}$ and averaged over the domain between $y = -3500$ and $+3500 \text{ km}$ (see text).

isentropic mass transport by remapping the flow field into isentropic coordinates and integrating up to the buoyancy b_i at which the mass transport $\overline{h_b v}$ changes sign:

$$\Psi_Q \equiv - \int_{b_{\min}}^{b_i} \overline{h_b v}(y, b') db'. \quad (28)$$

We then calculated the mean isentropic mass transport over the baroclinic zone between $y = -3500$ and $+3500 \text{ km}$ for all simulations. The eddy diffusivity is calculated from the near-surface³ flux–gradient relationship for buoyancy as $D = -(\overline{v' b'^s} / \partial_y \overline{b'^s})$. Again mean values over the baroclinic zone between $y = -3500$ and $+3500 \text{ km}$ are presented for all simulations.

The resulting mean overturning mass transport and eddy diffusivity estimates are shown in Fig. 8. While both the isentropic mass transport and the eddy diffusivity

³ Because of the use of no-slip boundary conditions in the simulations discussed here, the actual eddy flux vanishes at the surface. We therefore evaluated the flux–gradient relationship to calculate the eddy diffusivity above the surface Ekman layer at 300-m height. Note that the theoretical predictions derived in section 3 assume a downgradient flux for the geostrophic eddy flux of surface buoyancy $\overline{v'_g b'^s}$, which is best approximated by the flux just above the Ekman layer.

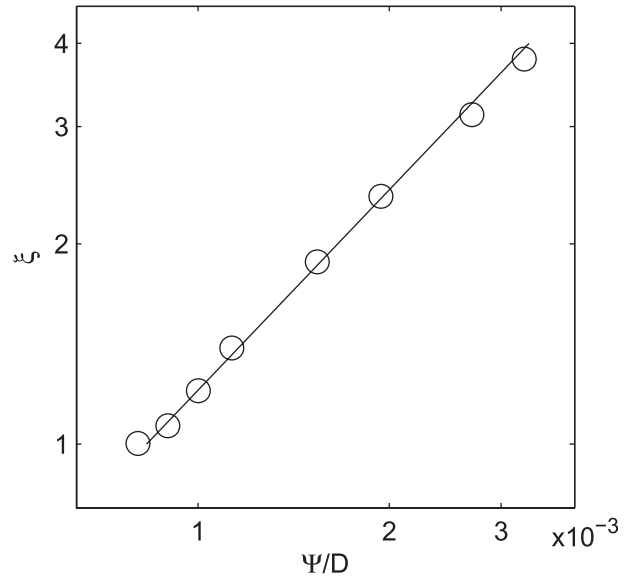


FIG. 9. Supercriticality ξ against the ratio of the isentropic mass transport and the eddy diffusivity Ψ/D . The black line denotes a slope of 1. All quantities are averaged over the baroclinic zone between $y = -3500$ and $+3500 \text{ km}$ (see text).

decrease as the thermal expansion coefficient is reduced, the eddy diffusivity decreases much more rapidly: the eddy diffusivity varies by a factor of about 15 over the range of simulations, while the isentropic mass transport changes only by about a factor of 3. In agreement with Eq. (16), this results in a steepening of the isentropes. Qualitatively, we can therefore understand the steepening of the isentropes as resulting from a reduction in the eddy diffusivity, which in turn is expected from the reduction of the deformation scale and baroclinicity with the thermal expansion coefficient.

The steepening of the isentropes here translates directly to an increase in the criticality parameter, since the latter varies much more than the height of the tropopause. Noting that the “planetary scale” β/f is also constant in the simulations shown here, the scaling for the criticality parameter is here dominated by changes in the isentropic slope (i.e., ξ is directly proportional Ψ_Q/D). As shown in Fig. 9, this is confirmed well by the numerical simulations.

c. Deriving a scaling relation for the criticality parameter

The scaling law for ξ can be made into a predictive theory, if Ψ_Q and D are expressed in terms of external parameters. Mixing length arguments (e.g., Pavan and Held 1996) suggest that the eddy diffusivity can be approximated by the product of the eddy scale and the barotropic eddy velocity, that is

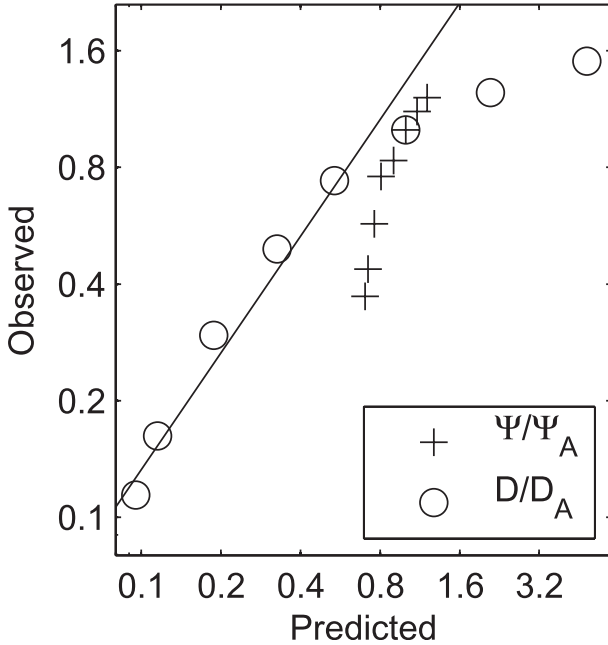


FIG. 10. Eddy diffusivity D against the scaling in Eq. (30) (circles), and isentropic mass transport Ψ against the inverse horizontal temperature gradient $(\partial_y \theta)^{-1}$ [see Eq. (31)]. All quantities are averaged over the baroclinic zone between $y = -3500$ and $+3500$ km and normalized by their respective values in the atmosphere-like simulation with $\alpha = 3.6 \times 10^{-3} \text{ K}^{-1}$. The black line denotes a slope of 1.

$$D \sim L_e \text{EKE}_t^{1/2}. \quad (29)$$

This scaling is shown to work in Fig. 8, and the eddy scale is well approximated by the Rhines scale in our simulations $L_e \approx L_\beta$ (Fig. 7). If we use the scaling $L_\beta \sim \xi L_d$ proposed by Held and Larichev (1996) for fully developed QG turbulence, we have

$$D \sim L_\beta \text{EKE}_t^{1/2} \sim L_\beta^3 \beta \sim \xi^3 \beta L_d^3. \quad (30)$$

While the first relation in Eq. (30) holds over the whole range of simulations, some caution must be used in applying Held and Larichev (1996)'s scaling relation because it is formally valid only for $L_\beta \gg L_d$ (i.e., for strongly supercritical simulations). Figure 10 shows that, despite the limited scale separation, the simulations broadly support the scaling in Eq. (30) as long as $\alpha < \alpha_A$ and $\xi > 1$. The scaling relation, however, breaks down for the marginally critical simulations with $\alpha \gtrsim \alpha_A$, which show much weaker eddy diffusivities than predicted by Eq. (30). A scaling for the isentropic mass transport was derived in section 3c, Eq. (14), as $\Psi_Q \sim (\Delta \bar{b}_{\text{eq}} / \partial_z \bar{b} \tau_r)$, where $\Delta \bar{b}_{\text{eq}}$ denotes the variation of the equilibrium buoyancy along the isentrope b_i , and l

denotes the distance between the latitudes where the isentrope b_i intersects with the surface and the tropopause. Using the fact that $l \sim (\bar{b}_z / \bar{b}_y) H_t$ and $b = g\alpha(\theta - \theta_0)$, we find that

$$\Psi_Q \sim \frac{\Delta \bar{b}_{\text{eq}} H_t}{\partial_y \bar{b} \tau_r} \sim \frac{\Delta \bar{\theta}_{\text{eq}} H_t}{\partial_y \bar{\theta} \tau_r}. \quad (31)$$

The scaling for the mass transport [Eq. (31)] has no explicit dependence on the thermal expansion coefficient, which is here varied much more strongly than any other mean-state variable. This explains why changes in the total isentropic mass transport are in general much smaller than changes in the eddy diffusivity, which instead depends explicitly on the thermal expansion coefficient via its dependence on the deformation scale per Eq. (30). The weak variations in Ψ_Q are dominated by variations in $\partial_y \bar{\theta}$ and $\Delta \bar{\theta}_{\text{eq}}$. Figure 10 shows the scaling [Eq. (31)], but considering only variations in Ψ_Q due to changes in $\partial_y \bar{\theta}$. This captures the variations in Ψ_Q well for simulations with $\alpha \geq 9 \times 10^{-4} \text{ K}^{-1}$, for which the isentropic slope changes little. The simulations with smaller α , however, show significantly weaker overturning circulations, which is due to the reduction in $\Delta \bar{\theta}_{\text{eq}}$ as the isentropes steepen (see Fig. 3). As we will show later, variations in $\Delta \bar{\theta}_{\text{eq}}$ are, however, negligible in the final scaling for the criticality parameter and can be ignored for present purposes. Notice also that the scaling [Eq. (31)] further assumes that the diabatic forcing is given by the radiative relaxation. An additional diabatic term arises from the convective adjustment scheme. This term is generally small compared to the heating associated with the relaxation scheme in our simulations.

We can now derive a scaling for the criticality parameter ξ in the supercritical regime in terms of mean state variables. Substituting Eqs. (31) and (30) back into Eq. (18) and rearranging terms yields

$$\xi \sim \left(\frac{1}{\tau_r f a \partial_y \bar{\theta}} \right)^{1/4} \left(\frac{L_d}{a} \right)^{-3/4}, \quad (32)$$

where $a = f/\beta$ denotes the dynamical planetary scale, which for our simulations (as well as for the earth's atmosphere) is comparable to the width of the baroclinic zone. Equation (32) predicts that variations in the criticality are dominated by variations in the deformation scale L_d , which decreases strongly as α is decreased. As confirmed by Fig. 11, we therefore find that the criticality parameter in the supercritical limit is to a good approximation proportional to the $-3/4$ th power of the deformation scale. Since the reduction in the deformation scale is dominated by the reduction in α , this qualitatively

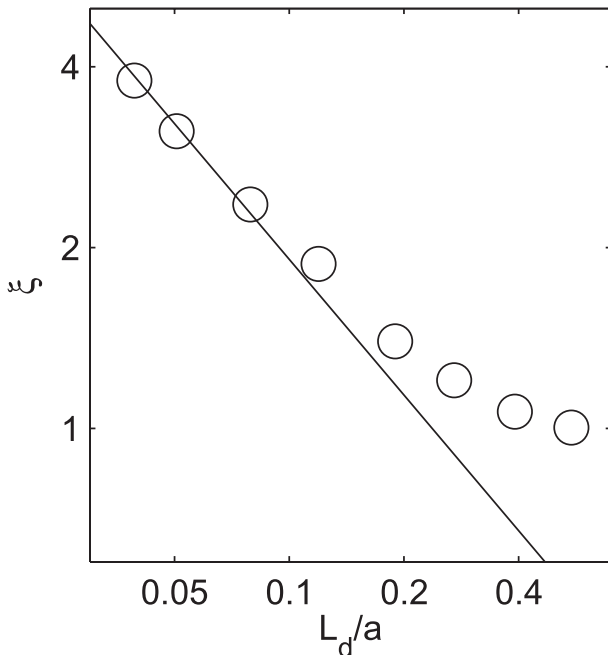


FIG. 11. Supercriticality ξ against the normalized deformation scale L_d/a [see Eq. (32)]. The black line denotes a slope of $-3/4$ (note that the axes are logarithmic). All quantities are averaged over the baroclinic zone between $y = -3500$ and $+3500$ km.

explains the observed increase in the criticality parameter as α is reduced. Since $\Delta\bar{\theta}_{eq}/a\partial_y\theta \sim O(1)$ and $\tau_r f \sim O(10^2)$, we may further note that the prefactor in Eq. (32) is on the order of $[(1/\tau_r f)(\Delta\bar{\theta}_{eq}/a\partial_y\theta)]^{1/4} \sim 0.2 - 0.4$. Equation (32) thus suggests that supercritical states may only be expected if $L_d/a \ll 1$, which is in general agreement with the results shown in Fig. 11.

The scaling [Eq. (32)] breaks down for simulations in which L_d/a becomes larger than about 0.2 and the criticality approaches one. The dependence of the criticality parameter on the deformation scale then flattens out and seems to asymptote toward a constant value close to one. This is in qualitative agreement with results from previous studies (e.g., Schneider 2004; Schneider and Walker 2006), who find that the criticality parameter of diabatically forced systems stays close to one over a wide range of parameters and forcings. The flattening out of the scaling relation between ξ and L_d/a is here associated dominantly with the breakdown of the diffusive scaling law [Eq. (30)], which is not expected to hold in the marginal critical limit and predicts much larger eddy diffusivities than observed in these simulations.

The saturation of the criticality parameter to one, for simulations where the Held and Larichev (1996) scaling relation breaks down, might seem to support traditional ideas of baroclinic adjustment. These predict that eddy activity will decrease rapidly once the criticality parameter

gets close to one because the system becomes neutral to baroclinic instability or unstable modes become shallow (e.g., Zurita-Gotor and Lindzen 2007, and references therein). Whether this reasoning is appropriate for the simulations presented here is, however, not clear. Preliminary simulations suggest that the breakdown of the Held and Larichev (1996) scaling for the eddy diffusivity is here at least partially associated with an increasing role of bottom friction in this limit, which might be via a direct influence of friction on the eddies themselves or indirectly via the modification of the mean flow and a “barotropic governor” mechanism (James and Gray 1986). The important role that bottom friction can play in controlling the eddy diffusivity has recently been discussed by Thompson and Young (2007). When and how exactly the transition to marginally critical states occurs, however, is beyond the scope of this study but will be the subject of future work.

It should also be noted that the eddy diffusivity scaling in Eq. (30) relies on the assumption that the eddy scale is proportional to the Rhines scale. However, our qualitative argument that the criticality increases for small α holds as long as the eddy diffusivity decreases as the thermal expansion coefficient is decreased. In the real ocean and atmosphere, where other processes (such as bottom friction) can prevent eddies from growing much beyond the deformation scale, Green (1970), Stone (1972), and many other authors since have proposed different scalings for the diffusivity. However, all these scalings share the property that the eddy diffusivity decreases as α is reduced.

Finally, one might ask whether there is a limit to the validity of the proposed scalings in the supercritical limit. One limitation comes from the assumption, implied in the scalings above, that the heat transport is dominated by large-scale eddies as opposed to convection, and that the stratification is dominantly statically stable. While this is true for all simulations discussed here, we do observe an increasing role of convection as the thermal expansion coefficient is reduced and the criticality increases, suggesting that there might be a limit where convective transports will start to dominate. Whether such a limit is universal or specific to a certain set of parameters and forcing, however, is an open question.

5. Summary and discussion

We showed that states with marginally critical as well as supercritical states with much steeper isentropic slopes can be obtained in a diabatically forced system if the thermal expansion coefficient is varied. Equilibrium states with criticality parameters close to one ($\xi \approx 1$) are found for large thermal expansion coefficients, which

are associated with deformation scales on the same order as the planetary scale. Supercritical mean states ($\xi > 1$) are obtained for small thermal expansion coefficients, which are associated with deformation scales much smaller than the planetary scale. As the thermal expansion coefficient is reduced, deformation-scale eddies become less effective at stabilizing the mean state, which causes an increase in the isentropic slope and thus in the criticality parameter. The higher criticality parameter allows for a more turbulent state with an upscale energy transfer from the scale of the instability to the Rhines scale due to nonlinear eddy–eddy interactions. In summary, in the marginally critical limit we find weakly nonlinear, deformation-scale eddies that are efficient in modifying the mean state. For supercritical states, instead, eddies are less efficient in modifying the mean state, but nonlinear eddy–eddy interactions become more important.

The results found in the limit of large thermal expansion coefficients resemble those observed in the real atmosphere, which is close to marginal criticality and dominated by weakly nonlinear eddies close to the deformation scale (e.g., O’Gorman and Schneider 2007, and references therein). The results found in the limit of small thermal expansion coefficients, on the other hand, display some of the characteristics found in the Southern Ocean, which is not in a state close to marginal criticality and where nonlinear eddy–eddy interactions are believed to be important in setting the observed eddy scale (e.g., Scott and Wang 2005). One difference, however, is that in the Southern Ocean the scale of the eddies is not generally set by the Rhines scale. This is likely because the upscale energy flux is arrested earlier by bottom drag and or topography.

The variations in the criticality parameter over our simulations are dominated by changes in the isentropic slope, which in turn are shown to be well captured by the scaling

$$s \sim \frac{\Psi_Q}{D}, \quad (33)$$

where Ψ_Q is the eddy-driven diabatic overturning circulation and D is the eddy diffusivity. We showed that the diabatic overturning is to first order independent of the thermal expansion coefficient. The scaling [Eq. (33)] therefore implies that the increase in criticality parameter for small expansion coefficients can be understood as stemming from a decrease in the eddy diffusivity as the deformation scale is reduced. In the limit of small thermal expansion coefficients, in which deformation scales are much smaller than the planetary scale, we can employ scalings for Ψ_Q and D to show that the criticality

parameter is to leading order proportional to the $-3/4$ th power of the deformation scale. In the limit of large thermal expansion coefficients (and deformation scales on the same order as the planetary scale), the criticality parameter asymptotes to a constant value close to unity. This latter limit is in agreement with previous studies that suggested that the atmosphere maintains a criticality parameter close to unity over a wide range of forcings and parameters, although the exact mechanisms responsible for this result remain unclear and will be subject of a future study.

It is worth noting that our results imply that supercritical, more strongly turbulent states are found in the limit of weaker buoyancy contrast to which the system is restored (since $\Delta b = g\alpha\Delta\theta$). These states are also characterized by an overall weaker EKE. The nondimensional ratio of EKE to the square of the mean baroclinic shear does, however, increase with the criticality, as predicted by QG studies (Held and Larichev 1996).

Our results are in qualitative agreement with recent work by Zurita-Gotor and Vallis (2011), who also find that the criticality parameter exceeds one in the limit of weak equilibrium horizontal temperature gradients if the depth of the tropopause is constrained by the radiative restoring profile, as in our simulations. Our results are also consistent with results shown in Schneider and Walker (2006), if one compares appropriate sets of simulations. In most of the simulations discussed in Schneider and Walker (2006), the convective adjustment scheme restores to a finite stratification to mimic the stabilizing effects of moisture. In these simulations the adjustment scheme becomes active in the limit of small buoyancy gradients, and prevents the system from reaching supercritical mean states—the system becomes subcritical once the stratification is set by the convection scheme. However, the authors also perform a series of simulations in which convective adjustment restores to a convectively neutral profile, as in our simulations. In agreement with our results, these simulations suggest equilibration to supercritical mean states in the limit of small buoyancy gradients.

An alternative perspective to equilibration of jets in the ocean and atmosphere is provided by the theory of transient stable amplification and adjustment to a generalized marginally stable state (Farrell and Ioannou 2009, and references therein). The theory has so far been derived using the QG approximation and prescribes the vertical stratification. This is a major limit for applying the theory to our work whose focus is on the changes in stratification and deformation radius. Moreover, the eddy–eddy fluxes, which are crucial in setting the large-scale adjustment, are not predicted by the theory. A test of the parameterizations used to close the problem, as

well as a generalization of these ideas to primitive equation systems, would be a welcome contribution to the discussion.

Acknowledgments. We thank Paul O’Gorman, Alan Plumb, Isaac Held, and John Marshall for helpful comments and discussions. We would also like to thank Tapio Schneider and Eli Tziperman for very constructive reviews. This work was supported through NFS award OCE-0849233.

APPENDIX A

Deriving a Scaling for the Criticality in a Quasigeostrophic Framework

The scalings for the overturning circulation, derived in section 3 for the more general primitive equations, can be recovered in a qualitative way using the continuously stratified QG equations. We will first discuss dynamical constraints on the zonal momentum balance. To close the momentum budget we will then need a closure for the eddy fluxes and a constraint for the meridional overturning mass transport. Armed with these two closures, we will be able to relate the turbulently adjusted mean state to the applied forcing. For simplicity all arguments and simulations presented here will assume a QG Boussinesq fluid in a flat-bottomed reentrant channel configuration.

a. Dynamical constraint: The zonal momentum balance

We start from the zonal momentum balance, which in the QG transformed Eulerian mean (TEM) formulation can be written as

$$-f_0 \bar{v}^* = \overline{v'q'}, \tag{A1}$$

where $\bar{v}^* = -\partial_z \psi^*$ denotes the residual meridional velocity, with the residual streamfunction $\psi^* \equiv -\int_0^z \bar{v} dz' + (\overline{v'b'}/\partial_z b_0)$ and the reference buoyancy profile b_0 . The QG PV is $q = f_0 + \beta y + \zeta_g + f_0 \partial_z (b/\partial_z b_0)$, with ζ_g the geostrophic relative vorticity. Frictional forces have been ignored because they are weak in the simulations used in this study. Zonal averages are here taken at constant z . We can integrate Eq. (A1) from the surface (for simplicity here again assumed to be flat at $z = 0$) to some height z to get

$$f_0 \psi^*(z) = \int_0^z \overline{v'q'} dz' + f_0 \frac{\overline{v'b'}}{\partial_z b_0}(0), \tag{A2}$$

where we used the fact that $\psi^*(0) = \overline{v'b'}/\partial_z b_0(0)$.

Assuming a diffusive closure for the eddy fluxes of PV and surface buoyancy and ignoring the contribution of relative vorticity to the PV, we find

$$\psi^*(z) = -\int_0^z D \left(\frac{\beta}{f_0} + \partial_{yz} \frac{\bar{b}}{\partial_z b_0} \right) dz' - D \frac{\partial_y \bar{b}}{\partial_z b_0}(0). \tag{A3}$$

If z is chosen close to the surface so that we can assume that the eddy diffusivity is approximately constant over the regarded layer, we get

$$\psi^*(z) = D \left[s(z) - \frac{\beta}{f_0} z \right], \tag{A4}$$

where $s = -(\partial_y \bar{b}/\partial_z b_0)$. Equation (A4) is the QG analog of Eq. (9) and shows that the residual transport below any level z is proportional to the eddy diffusivity times the effective PV gradient vertically integrated below z . The latter is given by the sum of the vertical integral of the planetary vorticity gradient and the isentropic slope at the top of the layer, and thus bears close resemblance to the PV gradient in the bottom layer of a layered QG model.

If we choose z to be a small height just above the surface, the β term in Eq. (A4) can be neglected and we obtain a scaling for the isentropic slope near the surface:

$$s = \frac{\psi^*}{D}. \tag{A5}$$

Substituting expression (A5) for the slope into the definition of the supercriticality, we find

$$\xi \sim \frac{f}{\beta H_t} \frac{\psi^*}{D}, \tag{A6}$$

which is the QG analog of Eq. (18). For any given planet (f/β fixed), the supercriticality ξ thus depends on the relation between the residual overturning ψ^* (which, as shown in the following section, can be related directly to the diabatic forcing), the eddy diffusivity, and the depth of the troposphere.

b. Thermodynamic constraint: Isentropic mass budget

Similar to our discussion in section 3b, we want to relate the residual overturning streamfunction ψ^* to the diabatic forcing using the thermodynamic equation

$$\partial_t \bar{b} = -\partial_y \psi^* \partial_z b_0 + \bar{Q}, \tag{A7}$$

where $Q = db/dt$ is the diabatic forcing. In steady state, we can integrate Eq. (A7) horizontally to get

$$\psi^* = \int_{y_{\min}}^y \frac{\overline{Q}}{\partial_z b_0} dy' \approx - \int_y^{y_{\max}} \frac{\overline{Q}}{\partial_z b_0} dy', \quad (\text{A8})$$

where y_{\min} and y_{\max} denote the southern and northern boundaries, respectively, where ψ^* is assumed to vanish. Condition (A8) is the QG analog of Eq. (13); however, because of the assumption of horizontal isentropes, implicit in the QG equations, the along-isentrope integration in Eq. (13) becomes a horizontal integration over the entire width of the domain.

We can now derive a scaling for ψ^* based on Eq. (A8). We will assume that the diabatic forcing can be represented by a radiative relaxation—that is, $Q = -(b - b_{\text{eq}}/\tau_r)$, with a restoring time scale τ_r and an equilibrium buoyancy profile b_{eq} . This is the form of radiative forcing used in our simulations and in many idealized studies of the atmosphere (e.g., Held and Suarez 1994; Schneider 2004). Using Eq. (A8) we then find

$$\psi^* \sim \frac{QL}{\partial_z b_0} \sim \frac{(b - b_{\text{eq}})L}{\partial_z b_0 \tau_r}. \quad (\text{A9})$$

Here L denotes the width of the domain, which naturally replaces the length of the isentrope l appearing in the isentropic coordinate scaling, consistent with the assumption that the isentropic slope is weak compared to the aspect ratio, implied in the QG approximation. Equation (A9) is the QG analog to the scaling in Eq. (14). In the main paper, we further relate the thermal

disequilibrium $(b - b_{\text{eq}})$ to the variation of the equilibrium buoyancy along an isentrope Δb_{eq} . The argument, however, cannot be readily transferred to the QG framework.

APPENDIX B

Implications of the Vertical Structure of Eddy Diffusivity

If we are to allow for the eddy diffusivity to have some vertical structure, the closure relationships for the eddy fluxes become

$$\overline{\hat{v}\hat{P}^*} = -D(b)\partial_y \overline{P^*}, \quad \overline{v'_g b'_s{}^s} = -D_s \partial_y \overline{b_s^s}, \quad (\text{B1})$$

where $D_s = \overline{D(b)^s}$. Note that D can of course also have a y dependence, which is not made explicit here since all relationships hold locally at any given y . Substituting these closures in the vertically integrated momentum budget in Eq. (7) yields

$$\int_{b_{\min}}^{b_i} \overline{h_b v^*} db \approx \int_{b_{\min}}^{b_i} D(b) \frac{\overline{h_b} \partial_y \overline{P^*}}{\overline{P^*}} db + \frac{f}{\overline{P^*}(\overline{b_s^s})} D_s \partial_y \overline{b_s^s}. \quad (\text{B2})$$

Following the same steps used to derive Eq. (8), we can write the first term on the rhs of Eq. (B2) as

$$\begin{aligned} \int_{b_{\min}}^{b_i} D(b) \frac{\overline{h_b} \partial_y \overline{P^*}}{\overline{P^*}} db &\approx \int_{b_{\min}}^{b_i} D(b) \left(\overline{h_b} \frac{\beta}{f} - \partial_y \overline{h_b} + \frac{f}{\overline{P^*}} \partial_y \Pi \right) db \\ &= D_{\text{SL}} \int_{b_{\min}}^{b_i} \left(\overline{h_b} \frac{\beta}{f} - \partial_y \overline{h_b} \right) db + \int_{b_{\min}}^{b_i} D(b) \frac{f}{\overline{P^*}} \partial_y \Pi db \\ &\approx D_{\text{SL}} \left[\frac{\beta}{f} \overline{z}(b_i) - \partial_y \overline{z}(b_i) \right] - D_s \frac{f}{\overline{P^*}(\overline{b_s^s})} \partial_y \overline{b_s^s}, \end{aligned} \quad (\text{B3})$$

where we defined a bulk SL diffusivity:

$$D_{\text{SL}} \equiv \frac{\int_{b_{\min}}^{b_i} D(b) \left(\overline{h_b} \frac{\beta}{f} - \partial_y \overline{h_b} \right) db}{\int_{b_{\min}}^{b_i} \left(\overline{h_b} \frac{\beta}{f} - \partial_y \overline{h_b} \right) db}. \quad (\text{B4})$$

The weighting factor in the definition of the bulk SL eddy diffusivity can be written as $\overline{h_b}(\beta/f) - \partial_y \overline{h_b} = \overline{h_b}(\beta/f) - \mathcal{H}(b - b_s) \partial_y b_s + \delta(b - b_s) \partial_b z \partial_y b_s$ and is generally

dominated by the contribution of the (negative) surface buoyancy gradient over the SL (e.g., Schneider 2005). In practice D_{SL} can therefore be expected to be well approximated by the surface diffusivity D_s .

APPENDIX C

A Scaling for the Diabatically Forced Overturning

We here derive a scaling for the diabatically forced overturning Ψ_Q [Eq. (12)], which is set by the heating

integrated along the lower part of an isentrope, which has to be balanced by a similar cooling above:

$$\Psi_Q \equiv \int_{y_s}^y \overline{hQ}(y', b_i) dy' \simeq - \int_{y_s}^{y_t} \overline{hQ}(y', b_i) dy'. \quad (C1)$$

Here y_s and y_t denote the southernmost and northernmost latitudes at which the isentrope b_i is above the surface and below the tropopause, at any time and longitude (or alternatively the southern and northern boundaries of the domain). If, for simplicity, we assume that the stratification between the surface and the tropopause changes little along b_i , then we can approximate Eq. (C1) as

$$\Psi_Q \approx \partial_z \bar{b}^{-1} \int_{y_s}^y \overline{Q}(y', b_i) dy' \approx -\partial_z \bar{b}^{-1} \int_{y_s}^{y_t} \overline{Q}(y', b_i) dy'. \quad (C2)$$

We now want to choose b_i such that it separates the regions of heating (below) and cooling (above)—that is, such that $Q(y', b_i) > 0$ for $y' < y$ and $Q(y', b_i) < 0$ for $y' > y$ (choosing b_i just above the SL generally fulfills this condition to a good approximation, since diabatic heating is usually confined to the SL while cooling is found above). We then find that

$$\Psi_Q \approx \frac{1}{2} \partial_z \bar{b}^{-1} \int_{y_s}^{y_t} |\overline{Q}(y', b_i)| dy'. \quad (C3)$$

Assuming a restoring condition such that $Q = -(b_i - b_{eq})/\tau_r$, where b_{eq} denotes the radiative equilibrium buoyancy and τ_r the restoring time scale, we get

$$\begin{aligned} \Psi_Q &\approx \frac{1}{2} \partial_z \bar{b}^{-1} \int_{y_s}^{y_t} \overline{\tau_r^{-1} |b_{eq} - b_i|} dy' \\ &= \frac{1}{2} \partial_z \bar{b}^{-1} \int_{y_s}^{y_t} \overline{\tau_r^{-1} |b_{eq} - \langle b_{eq} \rangle|} dy', \end{aligned} \quad (C4)$$

where $\langle \bar{b}_{eq} \rangle \equiv \int_{y_s}^{y_t} \overline{\tau_r^{-1} b_{eq}} dy / \int_{y_s}^{y_t} \overline{\tau_r^{-1}} dy$ is the weighted mean equilibrium buoyancy along the isentrope b_i , and we again used that the net heating over b_i vanishes. We thus find that the residual overturning mass flux scales as

$$\Psi_Q \sim \frac{\Delta b_{eq} l}{\partial_z \bar{b} \tau_r}, \quad (C5)$$

where Δb_{eq} denotes the variation of the equilibrium buoyancy over b_i , and l denotes the length of the isentrope between the surface and the tropopause.

APPENDIX D

The Spectral EKE Budget

We showed in Fig. 7 that the separation between the scale of the eddies (which scales with the Rhines scale) and the scale of the instability (which scales with the deformation scale) increases as the thermal expansion coefficient is reduced. This suggests that our simulations must display a substantial upscale transfer of eddy kinetic energy from the scale of the instability to the Rhines scale for small α . To support this conclusion we compute the spectral eddy kinetic energy budget for the two simulations with the largest and smallest thermal expansion coefficients. We calculate the vertically integrated eddy kinetic energy budget in terms of horizontal wavenumbers. The calculation is analog to Koshyk and Hamilton (2001) except that, because of the Cartesian geometry underlying our simulations, we use horizontal wavenumbers instead of spherical harmonics. We further separate the EKE and KE of the zonal mean flow, an important distinction for our purposes.

The spectral EKE budget can then be written as

$$\partial_t \text{EKE}_K \approx T_{EE} - T_{EM} + T_{PK} - D, \quad \text{where} \quad (D1)$$

$$\text{EKE}_K = \left\langle \int_0^H \frac{1}{2} (|u'_K|^2 + |v'_K|^2) dz \right\rangle, \quad (D2)$$

denotes the EKE at the horizontal wavenumber $K = \sqrt{k^2 + l^2}$, with the angle brackets here denoting a time mean,

$$T_{EE} = \left\langle \int_0^H \text{Re}[-u_K'^* (\mathbf{u}' \cdot \nabla u')_K - v_K'^* (\mathbf{u}' \cdot \nabla v')_K] dz \right\rangle \quad (D3)$$

denotes the spectral eddy–eddy energy transfer,

$$\begin{aligned} T_{EM} = \left\langle \int_0^H \text{Re}[u_K'^* (\mathbf{u}' \cdot \nabla \bar{u})_K + v_K'^* (\mathbf{u}' \cdot \nabla \bar{v})_K \right. \\ \left. + u_K'^* (\bar{\mathbf{u}} \cdot \nabla u')_K + v_K'^* (\bar{\mathbf{u}} \cdot \nabla v')_K] dz \right\rangle \end{aligned} \quad (D4)$$

denotes the spectral kinetic energy transfer from the eddies to the mean flow,

$$T_{PK} = \left\langle \int_0^H \text{Re}(w_K'^* b'_K) dz \right\rangle \quad (D5)$$

denotes the energy transfer from eddy available potential energy to eddy kinetic energy, and

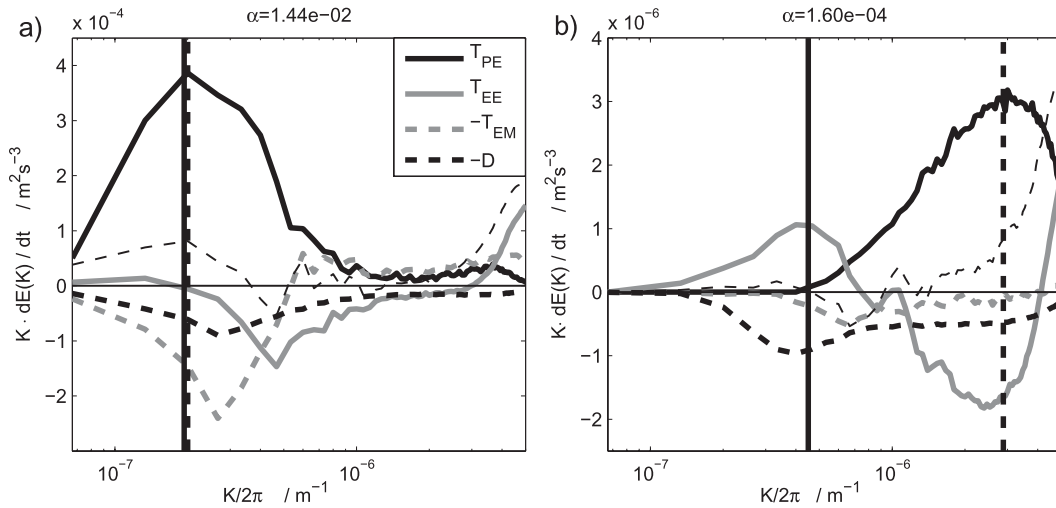


FIG. D1. (a) Spectral EKE budget for the simulation with $\alpha = 1.44 \times 10^{-2} \text{ K}^{-1}$: eddy APE to EKE transfer (solid black), EKE transfer due to eddy–eddy interactions (solid gray), mean KE to EKE transfer (dashed gray), and the explicit part of the dissipation (dashed black). The kinetic energy transfer terms have been smoothed by a five-point running mean. The thin dashed black line denotes the residual and includes the dissipation due to the numerical filter, which becomes dominant near the grid scale. Note that the residual, which (next to the numerical filter) arises from limited statistics and inaccuracy in the calculation of the spectral transfer terms, is small compared to the leading-order terms at all relevant wavenumbers away from the grid scale. The vertical black dashed and solid lines denote the Rhines scale and the scale of the instability, respectively, which are shown in Fig. 7. (b) As in (a), but for the simulation with $\alpha = 1.6 \times 10^{-4} \text{ K}^{-1}$.

$$D = \left\langle \int_0^H \text{Re}(u_K'^* \nu \partial_{zz} u_K' + v_K'^* \nu \partial_{zz} v_K') dz \right\rangle + \text{filter} \quad (\text{D6})$$

denotes dissipation by the explicit vertical viscosity ν and by the numerical filter (Shapiro 1970). Note that there is some contribution to the energy budget at any given wavenumber by the Coriolis term because f is not constant with latitude. This term, however, is small in our simulations and is herein ignored.

Figure D1 shows all the terms in the spectral EKE budget for the two simulations with the largest and smallest thermal expansion coefficients $\alpha = 1.44 \times 10^{-2}$ and $1.6 \times 10^{-4} \text{ K}^{-1}$. In both experiments the transfer from eddy APE to EKE peaks at the scale of instability as calculated from the QG instability analysis and shown in Fig. 7. For the simulation with the largest thermal expansion coefficient $\alpha = 1.44 \times 10^{-2} \text{ K}^{-1}$, this instability scale coincides with the Rhines scale, and thereby with the dominant barotropic eddy scale. The EKE produced at the scale of the instability is therefore dominantly transferred into the mean flow or dissipated in eddies of similar scales. No significant upscale eddy–eddy transfer is observed, although some energy is transferred to small scales where it is dissipated by the numerical filter. For the simulation with the smallest thermal expansion coefficient $\alpha = 1.6 \times 10^{-4} \text{ K}^{-1}$, the

instability scale is significantly smaller (by about a factor of 6) than the Rhines scale, which in turn coincides with the dominant barotropic eddy scale. The EKE at this larger scale is maintained by an upscale energy transfer from the scale of the instability to the Rhines scale. The transfer of kinetic energy from the eddies to the mean flow plays a smaller role in this simulation.

The results presented here support the conclusion presented in the main paper that, while the simulations with large thermal expansion coefficients are marginally critical and do not exhibit a significant upscale transfer of EKE, the simulations with the smallest thermal expansion coefficients show all aspects of a supercritical state, including a significant upscale energy transfer that is responsible for setting the scale of the barotropic eddies. The upscale energy transfer here spans about a factor of 6 in wavenumber space, which is of similar order though likely somewhat larger than found in the Southern Ocean (e.g., Tulloch et al. 2011). Notice that even though upscale energy fluxes due to nonlinear eddy–eddy interactions are important for the dynamics in these states, we do not find a clean “inertial range” over which the energy flux is constant and unaffected by EKE production or dissipation. Such an inertial range can be achieved only if the scale separation between the maximum EKE production and dissipation (or transfer to the mean flow) spans several orders of magnitude. Given our computational resources, we cannot run simulations

spanning such a wide range of scales, nor does such a limit appear to be relevant for the ocean or the atmosphere.

REFERENCES

- Barry, L., G. C. Craig, and J. Thuburn, 2000: A GCM investigation into the nature of baroclinic adjustment. *J. Atmos. Sci.*, **57**, 1141–1155.
- Bartels, J., D. Peters, and G. Schmitz, 1998: Climatological Ertel's potential-vorticity flux and mean meridional circulation in the extratropical troposphere–lower stratosphere. *Ann. Geophys.*, **16**, 250–265.
- Farrell, B. F., and P. J. Ioannou, 2009: A theory of baroclinic turbulence. *J. Atmos. Sci.*, **66**, 2444–2454.
- Green, J. S. A., 1970: Transfer properties of the large-scale eddies and the general circulation of the atmosphere. *Quart. J. Roy. Meteor. Soc.*, **96**, 157–185.
- Held, I. M., 1978: The vertical scale of an unstable baroclinic wave and its importance for eddy heat flux parameterizations. *J. Atmos. Sci.*, **35**, 572–576.
- , 1982: On the height of the tropopause and the static stability of the troposphere. *J. Atmos. Sci.*, **39**, 412–417.
- , and M. J. Suarez, 1994: A proposal for the intercomparison of the dynamical cores of atmospheric general circulation models. *Bull. Amer. Meteor. Soc.*, **75**, 1825–1830.
- , and V. D. Larichev, 1996: A scaling theory for horizontally homogeneous baroclinically unstable flow on a beta plane. *J. Atmos. Sci.*, **53**, 946–952.
- , and T. Schneider, 1999: The surface branch of the zonally averaged mass transport circulation in the troposphere. *J. Atmos. Sci.*, **56**, 1688–1697.
- James, I. N., and L. J. Gray, 1986: Concerning the effect of surface drag on the circulation of a baroclinic planetary atmosphere. *Quart. J. Roy. Meteor. Soc.*, **112**, 1231–1250.
- Karsten, R., and J. Marshall, 2002: Constructing the residual circulation of the ACC from observations. *J. Phys. Oceanogr.*, **32**, 3315–3327.
- Koh, T.-Y., and R. A. Plumb, 2004: Isentropic zonal average formalism and the near-surface circulation. *Quart. J. Roy. Meteor. Soc.*, **130**, 1631–1653.
- Koshyk, J. N., and K. Hamilton, 2001: The horizontal kinetic energy spectrum and spectral budget simulated by a high-resolution troposphere–stratosphere–mesosphere GCM. *J. Atmos. Sci.*, **58**, 329–348.
- Marshall, J., and T. Radko, 2003: Residual mean solutions for the Antarctic Circumpolar Current and its associated overturning circulation. *J. Phys. Oceanogr.*, **33**, 2341–2354.
- , C. Hill, L. Perelman, and A. Adcroft, 1997: Hydrostatic, quasi-hydrostatic, and nonhydrostatic ocean modeling. *J. Geophys. Res.*, **102**, 5733–5752.
- Merlis, T. M., and T. Schneider, 2009: Scales of linear baroclinic instability and macroturbulence in dry atmospheres. *J. Atmos. Sci.*, **66**, 1821–1833.
- O'Gorman, P. A., and T. Schneider, 2007: Recovery of atmospheric flow statistics in a general circulation model without nonlinear eddy–eddy interactions. *Geophys. Res. Lett.*, **34**, L22801, doi:10.1029/2007GL031779.
- Panetta, R. L., and I. M. Held, 1988: Baroclinic eddy fluxes in a one-dimensional model of quasi-geostrophic turbulence. *J. Atmos. Sci.*, **45**, 3354–3365.
- Pavan, V., and I. Held, 1996: The diffusive approximation for eddy fluxes in baroclinically unstable jets. *J. Atmos. Sci.*, **53**, 1262–1272.
- Rhines, P., and W. Young, 1982: Homogenization of potential vorticity in planetary gyres. *J. Fluid Mech.*, **122**, 347–367.
- Schneider, T., 2004: The tropopause and the thermal stratification in the extratropics of a dry atmosphere. *J. Atmos. Sci.*, **61**, 1317–1340.
- , 2005: Zonal momentum balance, potential vorticity dynamics, and mass fluxes on near-surface isentropes. *J. Atmos. Sci.*, **62**, 1884–1900.
- , and C. C. Walker, 2006: Self-organization of atmospheric macroturbulence into critical states of weak nonlinear eddy–eddy interactions. *J. Atmos. Sci.*, **63**, 1569–1586.
- , and J. Liu, 2009: Formation of jets and equatorial super rotation on Jupiter. *J. Atmos. Sci.*, **66**, 579–601.
- Scott, R., and F. Wang, 2005: Direct evidence of an oceanic inverse kinetic energy cascade from satellite altimetry. *J. Phys. Oceanogr.*, **35**, 1650–1666.
- Shapiro, R., 1970: Smoothing, filtering, and boundary effects. *Rev. Geophys. Space Phys.*, **8**, 359–387.
- Smith, K. S., 2007: The geography of linear baroclinic instability in Earth's oceans. *J. Mar. Res.*, **65**, 655–683.
- Stone, P. H., 1972: A simplified radiative-dynamical model for the static stability of rotating atmospheres. *J. Atmos. Sci.*, **29**, 405–418.
- , 1978: Baroclinic adjustment. *J. Atmos. Sci.*, **35**, 561–571.
- Thompson, A. F., and W. R. Young, 2007: Two-layer baroclinic eddy heat fluxes: Zonal flows and energy balance. *J. Atmos. Sci.*, **64**, 3214–3231.
- Thuburn, J., and G. C. Craig, 1997: GCM tests of theories for the height of the tropopause. *J. Atmos. Sci.*, **54**, 869–882.
- Tulloch, R., J. Marshall, C. Hill, and K. S. Smith, 2011: Scales, growth rates and spectral fluxes of baroclinic instability in the ocean. *J. Phys. Oceanogr.*, **41**, 1057–1076.
- Wunsch, C., and R. Ferrari, 2004: Vertical mixing, energy, and the general circulation of the oceans. *Annu. Rev. Fluid Mech.*, **36**, 281–314.
- Zurita-Gotor, P., 2008: The sensitivity of the isentropic slope in a primitive equation dry model. *J. Atmos. Sci.*, **65**, 43–65.
- , and R. S. Lindzen, 2007: Theories of baroclinic adjustment and eddy equilibration. *The Global Circulation of the Atmosphere*, T. Schneider and A. H. Sobel, Eds., Princeton University Press, 22–46.
- , and G. K. Vallis, 2011: Dynamics of midlatitude tropopause height in an idealized model. *J. Atmos. Sci.*, **68**, 823–838.